site $CB_{coastal\_1}$) indicate that biogenic opal increases in an inshore direction (from 10 to 17% of total flux at sites $CB_{coastal\_1}$ and CB_14, respectively) but is still not the dominant contributor to total mass fluxes. This change effects oceanic PCO_2 via the carbon rain ratio and the biological pump. PCO_2 measurements in a reasonable temporal and spatial resolution as done for the Oregon coastal region (Hales et al., 2005) are not accessible from the NW African margin, in particular not from coastal environments (Takahashi et al. 2002). Especially the larger filaments (e.g. off Cape Blanc, Cape Ghir and Cape Bojador) are complex structures and require detailed investigations at several E-W and N-S transects before defining CO_2 sources and sinks on seasonal and annual timescales. If and how the coastal upwelling system off NW Africa reacts to larger scale climatic variations such as the NAO and the ENSO is yet another important issue, also with respect to upwelling of nutrients, oceanic PCO_2, carbon export and sequestration.

Ocean margins are a significant source of organic matter for the deep ocean (e.g. Bauer and Druffel, 1998). *Lateral advection* processes, however, which export organic carbon from the shelf to the continental margins and the deep sea (e.g. Neuer et al., 1997; Helmke et al., 2005) are presently not well understood. Vertical and horizontal transport of particulate matter off NW Africa, for instance, is described by Ratmeyer et al. (1999a) for three sites CI, CB and CV, using grain size analysis of the lithogenic fraction at different trap levels. From these studies, it can be shown that material is advected and scavenged in the deeper water column at the ESTOC site, despite relatively fast settling velocities of larger particles. At site CB, however, the vertical transfer of particles seems to be fast and fairly undisturbed. A different transport mechanism was found for site CV in the Guinea Dome, suggesting different source areas for upper and lower traps. High-resolution modelling of particle transport in the water column is essential to understand the complex sedimentation processes at continental margins and to establish budgets for the modern cross-shelf export of organic carbon. Generally, horizontal transport processes appear to be very important and there is existing evidence of larger mass transports like slides, slumps, debris flows and turbidities in the entire area off NW Africa (e.g. Weaver et al., 2000).

2.6 Iberian Margin: The Rías[4]

Xosé Antón Álvarez-Salgado,
Alberto Vieira Borges,
Francisco Gómez Figueiras
and Lei Chou

2.6.1 The NW Iberian Upwelling System

The Iberian Upwelling System comprises the Atlantic coast of Portugal and Spain, from 37°N to 43°N (Fig. 2.6.1). It constitutes the northern limit of the upwelling system off Iberia–NW Africa associated with the eastern boundary Canary Current System (Wooster et al. 1976; Barton 1998). At these latitudes, coastal winds are seasonal (Fig. 2.6.2a): northerly winds prevail from March–April to September–October (upwelling season) and southerly winds predominate the rest of the year (downwelling season). However, this seasonal cycle explains <15% of the total variability of coastal winds and >70% of which concentrates in periods of less than 1 month. The upwelling season appears as a succession of wind stress/relaxation cycles of period 10–20 days (Blanton et al. 1987; Álvarez-Salgado et al. 1993) as in other coastal upwelling system at comparable latitudes (Hill et al. 1998).

The surface circulation of the northern Iberian basin is characterized by a year round weak southward flow (Peliz et al. 2005) known as the Portugal (PC) or Iberian current (IC; Fig. 2.6.1). Mazé et al. (1997) assumed that 10°30'W was the eastern boundary of the IC. East of that longitude and north of 40°N, a poleward-flowing slope current carries

X.A. Álvarez-Salgado (✉)
CSIC, Instituto de Investigacións Mariñas, Eduardo Cabello 6, 36208 Vigo, Spain
e-mail: xsalgado@iim.csic.es

[4] XAAS and FGF were funded by the Spanish MEC grants REN2002–02111/MAR and REN2003–06633–C03–02/MAR. AVB is a research associate at the FNRS. This is a contribution to the European Network of Excellence EUR–OCEANS (contract no. 511106–2) and European Integrated Project CARBO–OCEAN (contract no. 511176–2). This is MARE contribution no. XXX.

AQ31

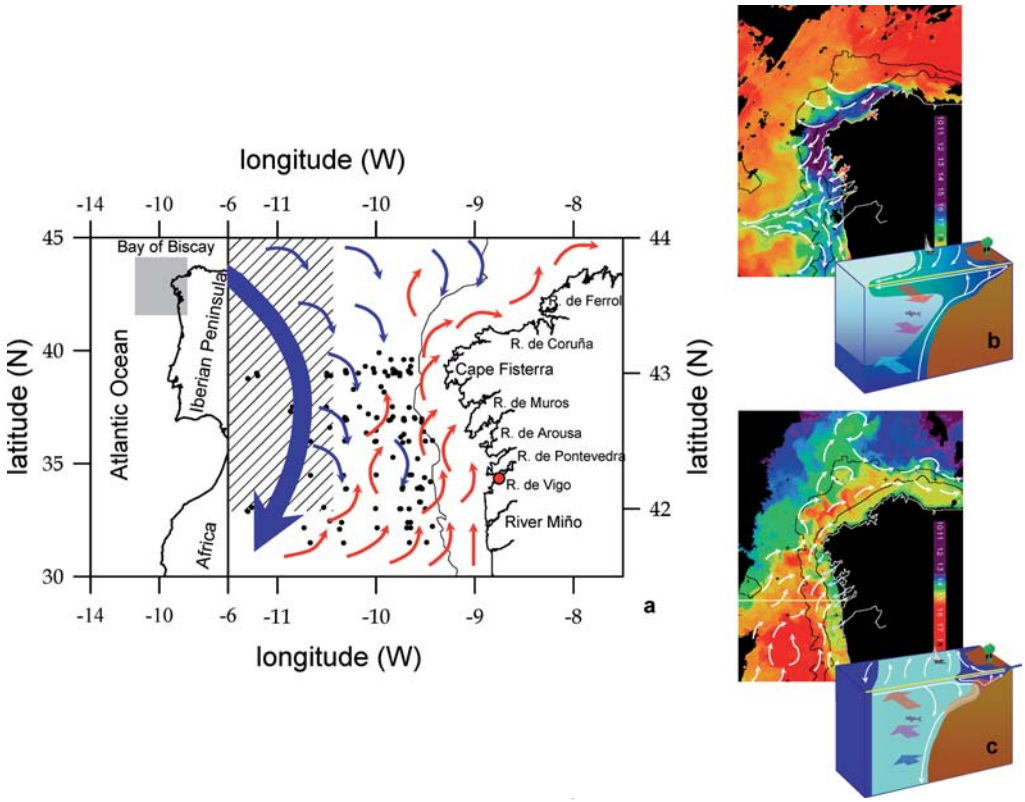

Fig. 2.6.1 (**a**) Map of the northwestern Iberian basin and the adjacent coastal zone, consisting of an open shelf and a system of large embayments freely connected with the shelf, known as rías. The oceanic Iberian Current (IC, *blue arrows*) and the slope Iberian Poleward Current (IPC, *red arrows*) are depicted. Striped area, 2° × 2° geostrophic cell centered at 43°N, 11°W where the offshore Ekman transport (rough estimate of the volume of water upwelled per km of coast) is calculated. *Red circle*, position of the time series station of the Ría de Vigo (40 m depth), sampled twice a week from 1987 to 1998. *Black circles*, position of the hydrographic stations sampled during different cruises to the northwestern Iberian basin to characterize the thermohaline and chemical properties of eastern North Atlantic Central Water. Schemes of the coupling between the 3D circulation of the open shelf and the 2D circulation of the rías under (**b**) upwelling and (**c**) downwelling conditions

warm, salty and nutrient-poor subtropical water along the Atlantic (Haynes and Barton 1990) and Cantabrian (Pingree and Le Cann 1990) coast of the Iberian Peninsula. It contrasts with the colder, fresher and nutrient-richer subpolar waters carried by the IC. During the upwelling season, north-easterly winds produce a southward-flowing surface current over the western Iberian shelf and slope (Torres et al. 2003) and the poleward flow drifts offshore and/or appears as a subsurface counter current (Peliz et al. 2005). In contrast, this poleward flow surfaces during the downwelling season in response to the predominant south westerly winds. It has been named Portugal Coastal Counter Current (PCCC, e.g. Álvarez-Salgado et al. 2003) or Iberian Poleward Current (IPC, e.g. García-Soto et al. 2002). The IPC is over 25–50 km wide and propagates at velocities of 15–30 cm s^{-1} (Martins et al. 2002; Huthnance et al. 2002).

The coastal wind pattern observed over the western Iberian shelf and slope also affects drastically the exchange with the Rías Baixas, four large (>2.5 km^3) coastal embayments that occupy the coastline between 42°N and 43°N (Fig. 2.6.1). During the upwelling season, when continental runoff is scarce, the rías act as an extension of the shelf (Rosón et al. 1997; Álvarez-Salgado et al. 2000). The 2D-positive residual circulation pattern of the rías (ingoing bottom current/outgoing surface current) responds to coastal winds at timescales ranging from a few hours to 2 days (Piedracoba et al. 2005). During the downwelling season, when continental runoff is high, the inner ría circulates as a positive estuary and the circulation of

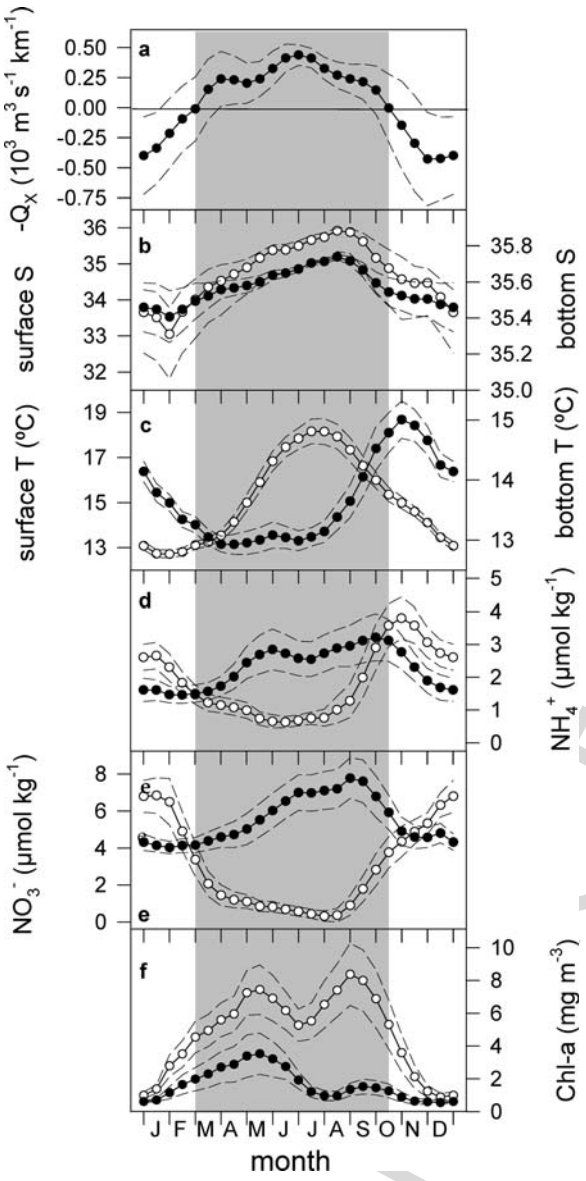

Fig. 2.6.2 Average ± SD seasonal cycles of (**a**) offshore Ekman transport ($-Q_X$) calculated in a $2^\circ \times 2^\circ$ geostrophic cell centered at 43°N 11°W (Fig. 2.6.1); (**b**) surface (2 m) and bottom (40 m) temperature (T), (**c**) salinity (S), (**d**) ammonium (NH_4^+), (**e**) nitrate (NO_3^-) and (**f**) chlorophyll *a* (Chl *a*) at the time series station of the Ría de Vigo (see Fig. 2.6.1), sampled twice a week from 1987 to 1998 (see Fig. 2.6.1). Offshore Ekman transport in 10^3 m^3 s^{-1} (km of coast)$^{-1}$, temperature in °C, ammonium and nitrate in µmol kg^{-1} and chlorophyll *a* in µg L^{-1}. *Open circles*, surface samples. *Solid circles*, bottom samples. Adapted from Nogueira et al. (1997)

the outer ría reverses (outgoing bottom current/ingoing surface current) in response to the prevailing southerly winds. The position of the convergence front between the positive circulation of the inner ría and the negative circulation of the outer ría depends on the relative strength of continental runoff and coastal winds (Álvarez-Salgado et al. 2000). The patch of fresh and cold water on the coastal side of the front, enriched in continental waters, is called the Western Iberian Buoyant Plume (WIBP; Peliz et al. 2005). The morphology of the rías, V shaped and with a unique open boundary, allows one to estimate reliable fluxes and budgets of carbon and nutrients by applying simplified 2D box models (e.g. Prego 1993, 1994, 2002). In addition, the closeness of the land-based laboratories and the protection against rough coastal winds allow intensive samplings to be conducted, overcoming the well-documented non-stationary behaviour of the rías (e.g. Álvarez-Salgado et al. 1996, 2001; Rosón et al. 1999; Pérez et al. 2000).

2.6.2 Hydrography of the Iberian Basin

Eastern North Atlantic Central Water (ENACW), modified in the surface layer by heat exchange with the atmosphere and continental runoff, characterizes the rías and the adjacent shelf. Two ENACW branches are observed in the area (Fiúza 1984; Ríos et al. 1992; Varela et al. 2005): (1) subtropical ENACW, formed to the south of 40°N in winter mixed layers of <150 m and transported northwards by the IPC and (2) subpolar ENACW, formed to the north of 45°N in winter mixed layers of >400 m and transported southwards by the IC. ENACW in the northern Iberian basin is characterized by a quasi-straight line in the θ/S diagram (Fig. 2.6.3a), ranging from a subsurface salinity maximum at 50–100 m depth, which surfaces during the winter mixing period, to a deep salinity minimum at 450–500 m depth (Pérez et al. 1993; Álvarez-Salgado et al. 2002). The isotherm of 13°C separates the warmer subtropical from the colder subpolar branches of ENACW. They present contrasting nutrient levels (Fig. 2.6.3b) because preformed nutrients are higher in the subpolar than in the subtropical waters (Pérez et al. 1993) and preferential mineralization of organic nitrogen and organic phosphorus compounds occurs in the subtropical ENACW domain (Castro et al. 2006). Both the subtropical and subpolar branches of ENACW upwell over the shelf and into the Rías Baixas, depending on the time of the year, and the

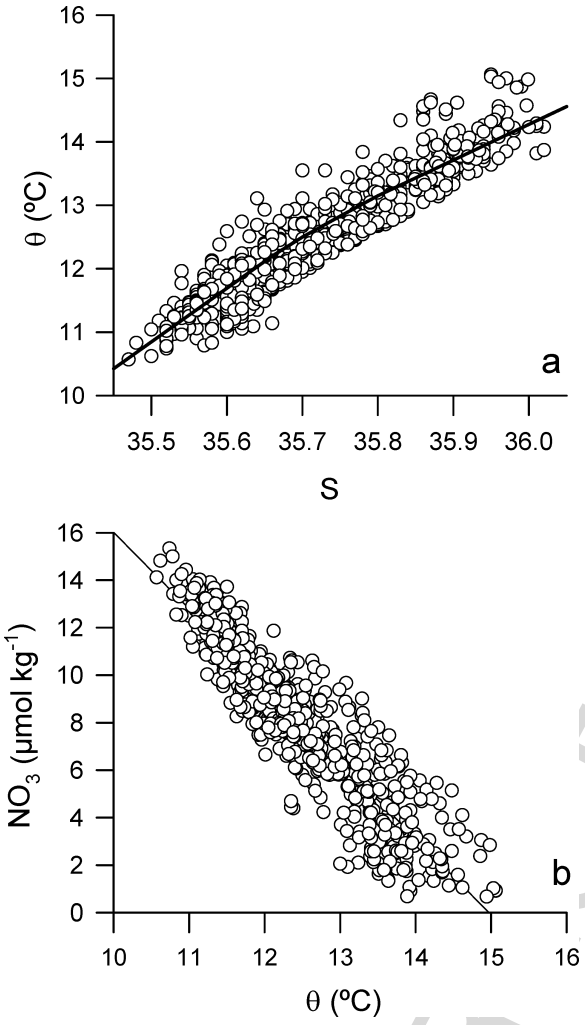

Fig. 2.6.3 (**a**) Potential temperature (θ) versus salinity (*S*) and (**b**) nitrate (NO_3^-) versus potential temperature (θ) plots of eastern North Atlantic Central Waters (ENACW) from the hydrographic stations sampled during different cruises to the northwestern Iberian basin shown in Fig. 2.6.1 (*solid circles*). Potential temperature in °C and nitrate in µmol kg^{-1}. Adapted from Álvarez-Salgado et al. (2002)

direction and intensity of coastal winds. A subsurface front is observed between the subtropical and subpolar ENACW (Fraga et al. 1982), which migrates seasonally from south of 42°N in April–May to north of 43°N in September–October (Castro 1997). In addition, during the intense upwelling events of July–August, water colder than 13°C enters the rías (Fig. 2.6.2b), indicating that the subpolar ENACW, that underlies subtropical ENACW, is promoted into the system.

It should be highlighted that nutrient levels carried by ENACW are 1/2–1/3 of those in the other major coastal upwelling systems (Arístegui et al. 2006). This is because the NW Iberian upwelling system is within the region of the ventilated thermocline of the eastern North Atlantic, in contrast with the aged central waters upwelled off NW and SW Africa, Peru, or California (Castro et al. 2000).

2.6.3 Hydrography of the Rías

The seasonal cycles of bottom temperature (Fig. 2.6.2b) and salinity (Fig. 2.6.2c) clearly show the effect of coastal winds (Fig. 2.6.2a) on the hydrography of the rías: 69% of the variability of bottom temperature is explained by coastal winds (Nogueira 1998), with minimum temperatures and maximum salinities coinciding with maximum offshore Ekman transport values during the upwelling season. In contrast, bottom temperatures are higher during the downwelling season, despite the corresponding colder autumn and winter months. The variability of surface temperature and salinity depends on coastal winds, which explains 78% of surface temperature, and on continental runoff, which explains 59% of surface salinity.

Ammonium (Fig. 2.6.2d) and nitrate (Fig. 2.6.2e) in bottom waters also follow the seasonal cycle of coastal winds, with maximum concentrations recorded during the upwelling season. It should be underlined that ammonium levels in the oceanic ENACW upwelled over the shelf are $<0.5\,\mu mol\,kg^{-1}$ (Álvarez-Salgado et al. 1997, 2002; Castro et al. 2000, 2006). Therefore, the high ammonium levels detected in the bottom ría are produced in situ as a consequence of intense ammonification processes. It is also remarkable that the ammonium maximum is recorded 1 month earlier than the nitrate maximum, suggesting a timescale for nitrification processes in the ría. Surface ammonium and nitrate concentrations show the expected seasonal cycle of spring/summer consumption and autumn/winter replenishment. Again, the surface nitrate maximum is delayed by about 1 month compared with the ammonium maximum.

Surface chlorophyll *a* (Fig. 2.6.2f) is characterized by minimum winter concentrations followed by spring and autumn maxima. These are the expected

seasonal cycles in any temperate marine system, except that summer chlorophyll *a* values remain relatively high because of the intermittent input of new nutrients by coastal upwelling (Figs 2.6.2d and e). It is remarkable that the spring and autumn maxima coincide with the transition from the downwelling to the upwelling favorable season and vice versa. Transitional periods are characterized by unstable meteorological conditions, with alternate wind directions. As suggested by Arístegui et al. (2006), the direction of prevailing winds (northerly versus southerly) during the spring and autumn maxima of chlorophyll *a* is highly indicative of their origin (in situ production versus accumulation) and fate (off-shelf export versus shelf sedimentation).

The seasonal cycle of phytoplankton (Fig. 2.6.4) consists of a winter period dominated by small phytoplankton forms and benthic diatoms succeeded by spring diatom and autumn dinoflagellate blooms; during summer there is a significant contribution from heterotrophic organisms (Figueiras and Ríos 1993). The different phytoplankton composition of spring and autumn blooms determines the contrasting seasonal evolution of chlorophyll in the surface and bottom layers (Fig. 2.6.2f). While the sinking of diatoms causes a conspicuous chlorophyll maximum in the bottom layer in spring, in autumn dinoflagellates are almost exclusively restricted to the surface. The convergence front between the positive circulation of the inner ría and the negative circulation of the outer ría during the downwelling season favors significantly the selection of dinoflagellates. The swimming ability of the latter allows them to remain afloat whilst diatoms are removed and exported to the shelf by the outgoing flow in the bottom layer (Figueiras et al. 1994; Fermín et al. 1996; Crespo et al. 2006). It should be highlighted that upwelling/downwelling cycles modify greatly the seasonal succession of phytoplankton. Thus, episodic strong northerly winds during the upwelling season reset the succession promoting the diatom growth (Fig. 2.6.5) as well as their export to the shelf (Tilstone et al. 1994, 2000). The subsequent wind relaxation or downwelling favors the appearance of dinoflagellates advected from the adjacent shelf (Margalef 1958; Tilstone et al. 1994; Pazos et al. 1995; Crespo et al. 2007).

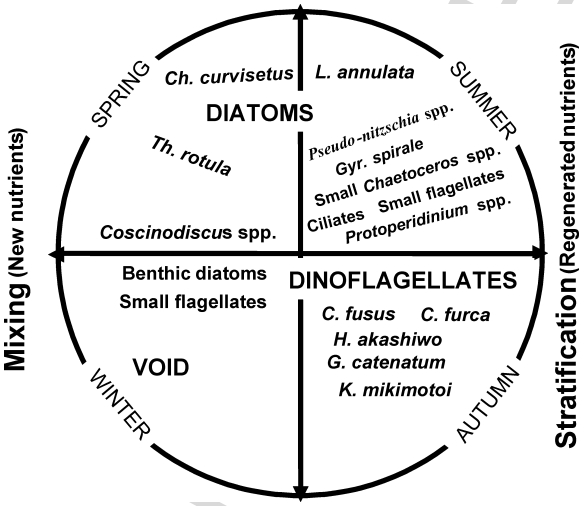

Fig. 2.6.4 Schematic representation of the phytoplankton succession in the Rías Baixas as a function of the season and the stratification/mixing conditions. The most representative species are shown. Adapted and simplified from Figueiras and Niell (1987)

Although the microplankton fraction (>20μm) dominates spring and autumn phytoplankton blooms in the rías (Tilstone et al. 1994; Cermeño et al. 2005, 2006; Lorenzo et al. 2005), nanoplankton (2–20 μm) is an important component of the phytoplankton biomass (~60%) in winter. Nano- and microphytoplankton (diatoms) are equally important during the upwelling season (Figueiras et al. 2002) with diatoms dominating at times of enhanced phytoplankton biomass (Cermeño et al. 2005, 2006). On the other hand, autotrophic picoplankton (<2μm) is a minor component of phytoplankton in the rías, accounting for 13 ± 10% of the total chlorophyll on an annual basis. This contribution, however, is higher when chlorophyll concentration is low, as is the case during winter (Rodríguez et al. 2003).

2.6.4 Fluxes and Budgets of Water, Carbon and Nitrogen Species in the Rías

Residual circulation patterns, as well as the associated fluxes of carbon and nitrogen species, and net ecosystem production (*NEP*) budgets have been evaluated for most of the Rías Baixas. At first, simple steady-state 2D box models were constructed following the Land–Ocean Interaction in the Coastal Zone (LOICZ) budgeting model (e.g. Prego 1993, 1994, 2002).

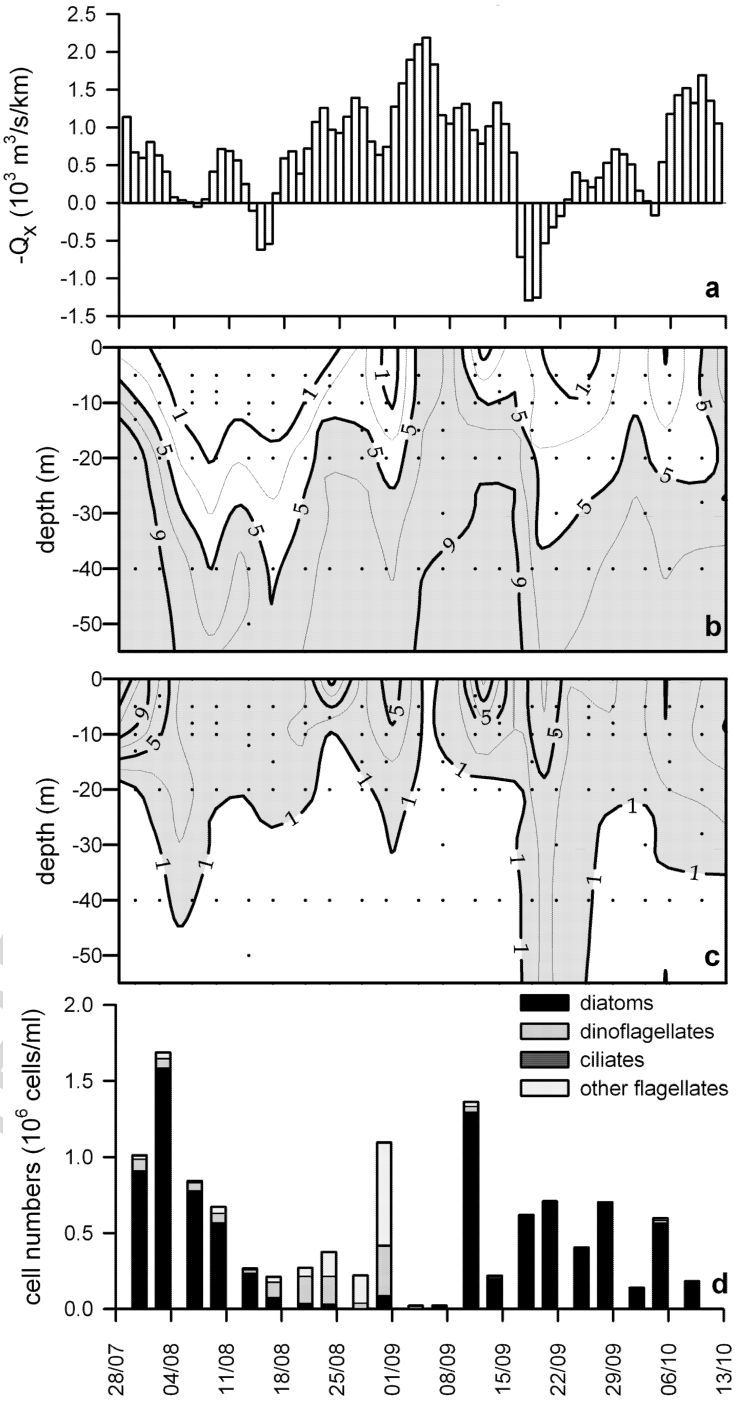

Fig. 2.6.5 (**a**) Offshore Ekman transport ($-Q_X$) calculated from the meridional wind component at Cape Fisterra (Fig. 2.6.1); profiles of (**b**) nitrate (NO_3^-) and (**c**) chlorophyll a (Chl *a*); and (**d**) diatom dinoflagellate, ciliate and other flagellate numbers in the central segment of the Ría de Arousa, from 28/07/89 to 13/10/89. Offshore Ekman transport in 10^3 m^3 s^{-1} (km of coast)$^{-1}$, nitrate in μmol kg^{-1} chlorophyll *a* in μg L^{-1} and cell numbers in 10^6 cell L^{-1}. Adapted from Pazos et al. (1995)

However, this steady-state approach was insufficient to explain the complex short-timescale dynamics of these coastal embayments. Therefore, intensive hydrographic surveys (one station per 25 km^2, twice a week) have been conducted in the rías to overcome this difficulty.

The time evolution of any variable, *C*, in the upper (photic) layer of the ría between two consecutive

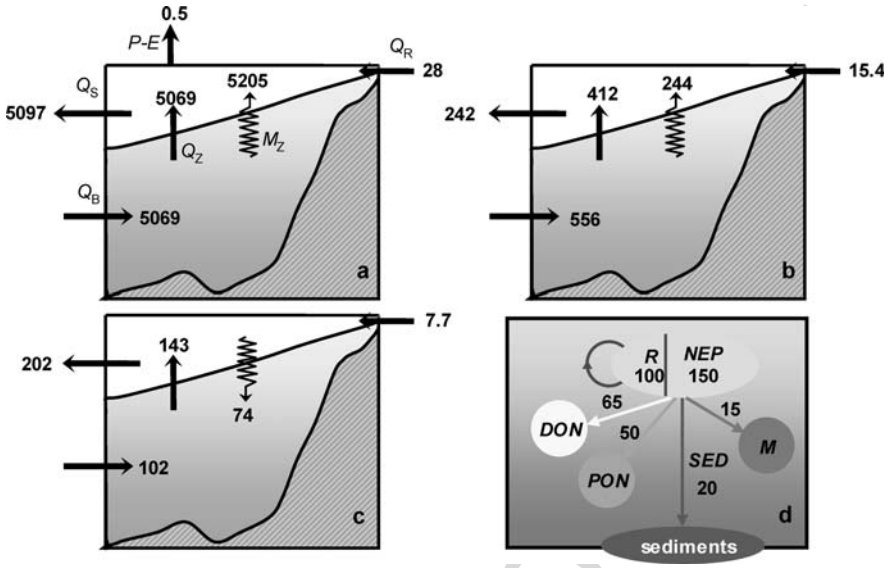

Fig. 2.6.6 (**a**) Water fluxes, (**b**) inorganic nitrogen and (**c**) particulate organic nitrogen fluxes, and (**d**) nitrogen biogeochemical budget for the Ría de Arousa during the upwelling season 1989. Q_S and Q_B are the horizontal surface and bottom convective flows at the outer boundary of the ría, respectively; Q_S and M_Z are the vertical convective and turbulent mixing flows, respectively; Q_R is the continental runoff; *NEP* and *R* are the net ecosystem production and respiration, respectively; *DON* and *PON* are the net export of dissolved and particulate organic nitrogen to the adjacent self; *M* is the net export of organic nitrogen associated with the extraction of mussels cultured on hanging ropes; and *SED* is the net export of organic nitrogen to the sediments of the ría. Water fluxes in $m^3\ s^{-1}$, nitrogen fluxes in $g\ N\ s^{-1}$, *NEP*, *R*, *M*, *DON*, *PON* and *SED* in $mg\ N\ m^2\ d^{-1}$ (a colored version of this figure is available online; see Appendix C)

surveys can be expressed by the following mass balance equation (Fig. 2.6.6a):

$$\frac{\Delta\,(V_U \cdot C_U)}{\Delta t} = Q_Z \cdot C_Z + M_Z \cdot (C_L - C_U) + Q_R \cdot C_R - Q_S \cdot C_S + ATM_C + NEP_C \quad (2.6.1)$$

where V_U is the volume of the upper layer (in m^3); Δt is the time step between two consecutive surveys (in s); C_U and C_L are the concentrations of C in the upper and lower layers, respectively (in mmol m^{-3}); C_S and C_Z are the concentrations of C in the outer and lower boundaries of the surface layer, respectively (in mmol m^{-3}); C_R is the concentration of C in continental runoff (in mmol m^{-3}); Q_Z and Q_S are the vertical and horizontal convective flows, respectively (in $m^3\ s^{-1}$); M_Z is the vertical turbulent mixing flow (in $m^3\ s^{-1}$); Q_R is the continental runoff (in $m^3\ s^{-1}$); ATM_C is the exchange of C with the atmosphere, including wet and dry deposition for dissolved chemicals and diffusion for gases (in mmol $m^{-3}\ d^{-1}$); NEP_C is the net ecosystem production of C, i.e. the autotrophic production minus the respiration of all autotrophs and heterotrophs in the study volume (Smith and Hollibaugh 1997). Q_R is obtained from gauging stations and Q_Z, Q_S and M_Z by solving simultaneously the system of mass balance equations for water, salinity and temperature ($NEP = 0$) of the upper and lower layers (see Rosón et al. 1997 for further details).

2.6.4.1 The Upwelling Season in the Rías

Figure 2.6.6a summarizes the averaged water flows in the Ría de Arousa from May to October 1989 (upwelling season) as derived from a series of 40 consecutive surveys spaced 3–4 days (Álvarez-Salgado et al. 1996; Rosón et al. 1999; Pérez et al. 2000). It is remarkable that 99.4% of the water that circulates in the ría comes from the adjacent shelf and continental waters supply only 0.6% of the water budget. It is also noticeable that the vertical advection and mixing flows are of quite comparable magnitude. As a consequence, 97% of the inorganic nitrogen (N_T) that enters the ría comes from the shelf and 3% from the rivers (Fig. 2.6.6b). An extra *NEP* of $100\ g\ s^{-1}$ of N_T occurs in the lower (aphotic) layer because of in situ pelagic and benthic nitrogen regeneration processes, i.e. the N_T flux to the upper layer is enriched by 18% compared with the ingoing bottom

flux from the shelf. Vertical advection transports to the photic layer 63% and turbulent mixing 37% of the N_T. Finally, comparison of the inputs and outputs indicates that the ría is able to trap efficiently 58% of the N_T that it receives, while releasing the remaining 42% to the shelf. On the contrary, the net export of particulate organic nitrogen (PON) corresponds to 100 g N s^{-1} (Fig. 2.6.6c), which is susceptible to sink and mineralize in shelf bottom waters. In fact, whereas the averaged N_T concentration of the bottom flow is 7.8 mmol m^{-3} (Fig. 2.6.6a and b) the expected N_T concentration of the ENACW in the adjacent ocean for the temperature of the bottom flow (Fig. 2.6.3b), 13.8°C minus the 0.5°C warming experienced during transit from the slope to the mouth of the ría (Álvarez-Salgado et al. 2002), should be 5.0 mmol m^{-3}. Therefore, there is a 54% N_T enrichment of the upwelled ENACW due to pelagic and benthic mineralization over the shelf. In conclusion, part of the N_T fertilization of the ría comes from mineralization of organic nitrogen exported from the ría itself, constituting a remarkable feedback process (Fraga 1981; Tenore et al. 1982; Fraga and Bakun 1993; Prego 1994). The proportion of mineralized nutrients increases through the upwelling season from 30% in May to 70% in October (Álvarez-Salgado et al. 1993) reaching maximum values at the mouth of the rías (Álvarez-Salgado et al. 1997). This is in agreement with the distribution of organic matter (López-Jamar et al. 1992) and biogenic silica (Prego and Bao 1997) found in shelf sediments.

The averaged *NEP* during the upwelling season is 150 mg N m^{-2} d^{-1} (Fig. 2.6.6d) with a O_2/C/N/P stoichiometry of 215/147/21/1 (Pérez et al. 2000). According to the stoichiometric model of Fraga (2001), it corresponds to the net synthesis of a (dry) material with elemental composition $C_{147}H_{238}O_{40}N_{21}P$, i.e. 53% w/w of proteins (average formula, $C_{147}H_{227}O_{46}N_{40}S$), 10% of phosphorus compounds ($C_{45}H_{76}O_{31}N_{12}P_5$), 32% of lipids ($C_{53}H_{89}O_6$) and 5% of carbohydrates ($C_6H_{10}O_5$). Therefore, the *NEP* in carbon units is 0.84 g C m^{-2} d^{-1}.

Pérez et al. (2000) were able to model the short-timescale (1/2 wk) variability of the *NEP* of the Ría de Arousa during the upwelling season (in mg N m^{-2} d^{-1}) as a function of three physical factors: the offshore Ekman transport (*E*), the heat exchange with the atmosphere (*F*) and the stability of the water column (Brunt–Väisälä frequency, *BV*):

$$NEP = 100(\pm 25) \cdot E_{-1} - 50(\pm 20) \cdot E_0 + 1.1(\pm 0.2) \cdot (F_0 + F_{-1/2}) - 285(\pm 50) \cdot BV_0$$
$$r = 0.84, n = 46, p < 0.001 \qquad (2.6.2)$$

where E_0 and E_{-1} are the offshore Ekman transports over the 1/2 week period when *NEP* is calculated and over the previous week, respectively (in m^3 s^{-1} (km of coast)$^{-1}$); F_0 and $F_{-1/2}$ are the heat exchange with the atmosphere over the 1/2 week period when *NEP* is calculated and over the previous 1/2 week period, respectively (in cal m^{-2} d^{-1}); and BV_0 is the Brunt–Väisälä over the 1/2 week period when *NEP* is calculated (min^{-1}).

Therefore, according to Eq. (2.6.2), 70% of the 1/2 week variability of *NEP* can be explained by a simple linear combination of physical parameters. It is remarkable that upwelling occurring over the previous week has a positive effect on *NEP* because of the fertilization with new nutrients, whereas upwelling occurring over the current 1/2 week has a negative effect because of the 'washing out' effect on the growing phytoplankton populations. The heat exchange with the atmosphere has a positive effect because of their direct relationship with the photosynthesis available radiation (PAR). The stability of the water column has a negative effect because stratification prevents the convective and diffusive upward transport of nutrients upwelled over the shelf and rías to the photic layer.

At the upwelling season timescale, about $^1/_3$ of the *NEP* (50 mg N m^{-2} d^{-1}) is exported to the adjacent shelf in the form of PON with a C/N molar ratio of 6.3 (Pérez et al. 2000). Extrapolation of the ratio of DOC/POC export of 1.3 obtained in the Ría de Vigo during the upwelling season 1997 (Gago et al. 2003a) yields a net export of DON to the adjacent shelf of 65 mg N m^{-2} d^{-1} (Fig. 2.6.6d). The intensive culture of mussels on hanging ropes in the Ría de Arousa extracts 10–15 mg N m^2 d^{-1} (Álvarez-Salgado et al. 1996) or 0.05–0.08 g C m^2 d^{-1} (Rosón et al. 1999) from the ría, i.e. 7–10% of *NEP*. Therefore, about 20–25 mg N m^2 d^{-1} is deposited over the sediments of the ría, corresponding to 13–17% of *NEP*.

Measurements of $H^{14}CO_3^-$ fixation rates in the central Ría de Arousa yielded an averaged primary production (*PP*) over the upwelling season of 1.50 g C m^{-2} d^{-1} or 250 mg N m^{-2} d^{-1} (Fig. 2.6.6d; Álvarez-Salgado et al. 1996). The difference between *PP* and *NEP* gives an ecosystem respiration rate (*R*) of

100 mg N m^{-2} d^{-1}. In summary, 40% of *PP* is respired within the water column of the ría and 60% is available for export to (1) higher tropic levels, essentially to mussels growing on hanging ropes (6% of *PP*), (2) the adjacent shelf, in the form of particulate (20% of *PP*) and dissolved (26% of *PP*) organic nitrogen; and (3) the sediments of the ría (8% of *PP*), which results in 2–3 wt.% of opal (Bernárdez et al. 2005) and 6–10 wt.% of organic matter (Vilas et al. 2005) in the sediments of the middle segment of the rías. The net accumulation of 8% of *PP* in the sediments of the ría at the upwelling season timescale is not comparable with the sedimentation rates obtained with traps moored at the base of the photic zone over short periods (normally 24 h), which could represent up to 75% of *PP* in the rías (Bode et al. 1998; Varela et al. 2003, 2004).

PP and *R* have been measured on a seasonal basis in the adjacent Ría de Vigo by the light/dark bottle incubation method (Moncoiffe 2000). The resulting averaged *PP* over the upwelling season of 1991 ranged from 2.0 to 2.5 g C m^{-2} d^{-1}, with 40% being respired in the photic zone and 25% in the aphotic zone. An averaged photic zone *R* of 44 ± 27% of *PP* was also obtained in the Ría de A Coruña by Teira et al. (2003) which is also consistent with the 33–43% contribution of ammonium regenerated by microheterotrophs to nitrogen uptake by phytoplankton in the same site (Bode et al. 2004). Therefore, 0.90–1.13 g C m^{-2} d^{-1} produced in the Ría de Vigo are available for export to higher trophic levels, the sediments of the ría and the adjacent shelf. This number is not far from the *NEP* of 0.84 g C m^{-2} d^{-1} obtained in the Ría de Arousa during the 1989 upwelling season. However, *PP* in the rías during the upwelling season is highly variable, ranging from <0.5 to >10 g C m^{-2} d^{-1} with a mean value of 2.5 ± 2.8 g C m^{-2} d^{-1} (Fraga 1976; Bode and Varela 1998; Tilstone et al. 1999; Teira et al. 2003; Varela et al. 2004, 2005; Lorenzo et al. 2005; Cermeño et al. 2006). Since the release of recently photosynthesized carbon in dissolved form appears to be a rather constant fraction (∼20%) of the total carbon fixation (Marañón et al. 2004, 2005), mean gross primary production (Pg) in the rías during the upwelling season can be estimated to be ∼3 g C m^{-2} d^{-1}.

At the 1/2 week timescale, low *PP* occurs during the wind stress or 'spin up' phase of strong upwelling events because of the previously referred 'washing out' effect. On the contrary, the highest *PP* values are measured during the wind relaxation or 'spin down' phase, when phytoplankton grows at the expenses of the previously upwelled nutrients and the off–shore export diminishes, favoring biomass accumulation in the rías. During this second phase, it is observed that *NEP* equals *PP* (i.e. *R* is nil), whereas *R* equals or exceeds *PP* during prolonged periods (>7 days) of calm wind or during downwelling events (i.e. the system is balanced or temporarily switched to heterotrophy). In the particular case of the Ría de Ferrol, connected to the shelf by a narrow channel, frequent phytoplankton blooms are not related to upwelling but to in situ nutrient regeneration of shelf surface waters retained inside the ría (Bode et al. 2005). On average, more than 65% of *PP* is due to the microphytoplankton fraction (>20 μm), although phytoplankton <20 μm can account for >50% of *PP* under transient low *PP* situations associated with strong upwelling conditions (Tilstone et al. 1999).

2.6.4.2 The Downwelling Season in the Rías

Information about carbon and nitrogen fluxes and *NEP* rates in the rías during the downwelling season is scarce. It concentrates mostly on September–October, because this is the time of the year when harmful dinoflagellate blooms usually occur (Fig. 2.6.2f). The existing information indicates that, despite the bloom conditions, this is a period of net heterotrophy (*Pg* < *R*). The excess respiration is supported by biogenic materials accumulated during productive upwelling events and fresh organic matter imported from the adjacent shelf, as a consequence of the reversal of the 2D residual circulation pattern (Álvarez-Salgado et al. 1996, 2001; Rosón et al. 1999; Gago et al. 2003b). In addition, the anomalous O_2/C/N/P stoichiometry obtained for the net ecosystem respiration of the Ría de Arousa during October 1989 (74/73/7.4/1; Pérez et al. 2000) suggests that anaerobic processes in the pelagic sediments should play a visible role when the ría switches to net heterotrophic conditions. Anaerobic processes are probably also active during the upwelling season, but they are overwhelmed by the dominant net production processes. The work by García-Gil et al. (2002) on shallow gas structures (likely methane) identified in the Ría de Vigo, as well as the denitrification activity measured by Dale and Prego (2002) in the sediments of the Ría de Pontevedra, supports this statement.

Carbon fluxes and *NEP* rates of the rías during the winter have been obtained only during two 1/2 month periods in December 1997 and February 2002, both in the Ría de Vigo. In the first study, evaluation of DOC fluxes and *NEP* rates indicates that active exchange with the adjacent shelf just affected the accumulation of semi-labile DOC within the study volume ($\Delta DOC/\Delta t$) rather than the *NEP* of labile DOC, which was nearly nil (Álvarez-Salgado et al. 2001). In the second study, a massive winter diatom bloom ($PP = 8.0\,\mathrm{g\,C\,m^{-2}\,d^{-1}}$) occurred during the relaxation period following a strong winter upwelling event. Most of the produced material was exported downwards to the sediments of the ría during the subsequent downwelling episode by a combination of advection and enhanced sedimentation rates (Álvarez-Salgado et al. 2005). Although, no clear pattern arises from the few observations made up to date, in general *PP* falls down well below $0.5\,\mathrm{g\,C\,m^{-2}\,d^{-1}}$, the lowest values reported for the upwelling season (Fraga 1976; Bode and Varela 1998; Teira et al. 2003; Varela et al. 2005; Cermeño et al. 2006). Occasionally, extremely low *PP* values, $<0.05\,\mathrm{g\,C\,m^{-2}\,d^{-1}}$, have been reported (Fraga 1976; Bode and Varela 1998). In addition, the existing time series of nutrient data suggest that net regeneration of ammonium and nitrate is not the cause of their accumulation in the surface layer from November to February (Fig. 2.6.2d and e). According to the levels of N nutrients in continental runoff to the Ría de Vigo ($35\,\mu\mathrm{mol\,L^{-1}}$; Pérez et al. 1992; Gago et al. 2005) and the proportion of freshwater in the surface layer, continental waters are able to account for excess of N nutrients in the surface layer as compared with the bottom layer, with regeneration representing <10% of the excess.

2.6.5 The Rías Versus the Open Adjacent Shelf

The 2D quasi-zonal circulation of the rías merges with the 3D quasi-meridional circulation of the middle and outer shelf (Fig. 2.6.1). The latter results mainly from the interaction of the basin-scale-driven IPC on the slope, the highly variable local winds acting on the Ekman layer, and the intricate topography of the NW Iberian coast. The complex landscape of the shoreline is partly responsible for the deformation of the IPC in the form of cool filaments during the upwelling season and Slope Water Oceanic EDDIES (SWODDIES) during the downwelling season (see reviews by Huthnance et al. 2002; Varela et al. 2005; Peliz et al. 2005). Note that both structures enhance the exchange of water and materials between the coastal transition zone (CTZ) and the adjacent ocean.

Based on existing information in the literature on carbon and nitrogen fluxes and biogeochemical rates, a carbon budget for the NW Iberian shelf during the upwelling season has been produced recently (Arístegui et al. 2006 and references therein). It is shown in Fig. 2.6.7 for comparison with the fluxes in the rías (Sect. 2.6.4.1). Despite their similar *PP* rates, the most striking differences between the rías and the adjacent shelf are that (1) whereas 46% of *PP* in the rías is exported to the shelf, only 20% of the shelf *PP* is exported to the open ocean; (2) pelagic mineralization represents 40% of shelf *PP* and only 25% of the rías *PP*; and (3) carbon burial is 1% of the shelf *PP* and as much as 8% of the rías *PP*.

Regarding the downwelling season, phytoplankton composition in shelf waters is characterized by the dominance of small forms and a negligible contribution of diatoms and dinoflagellates (Tilstone et al. 2003; Calvo-Díaz et al. 2004; Rodríguez et al. 2006; Crespo and Figueiras 2007). *PP* is in the order of the values reported for the rías, typically $<0.3\,\mathrm{g\,C\,m^{-2}\,d^{-1}}$ (Joint et al. 2002; Tilstone et al. 2003). However, knowledge on the carbon and nitrogen fluxes and *NEP* rates is still lacking for the downwelling season in NW Iberian shelf waters.

2.6.6 Carbon Dioxide (CO_2) Distribution and Exchange with the Atmosphere in Ría and Shelf Surface Waters of the NW Iberian Upwelling System

2.6.6.1 Distribution of pCO_2 in Surface Waters over the Shelf

The typical distribution of salinity, temperature and partial pressure of CO_2 (pCO_2) in the surface waters off the NW Iberian coast during winter and summer is shown in Fig. 2.6.8. During July 1998, active

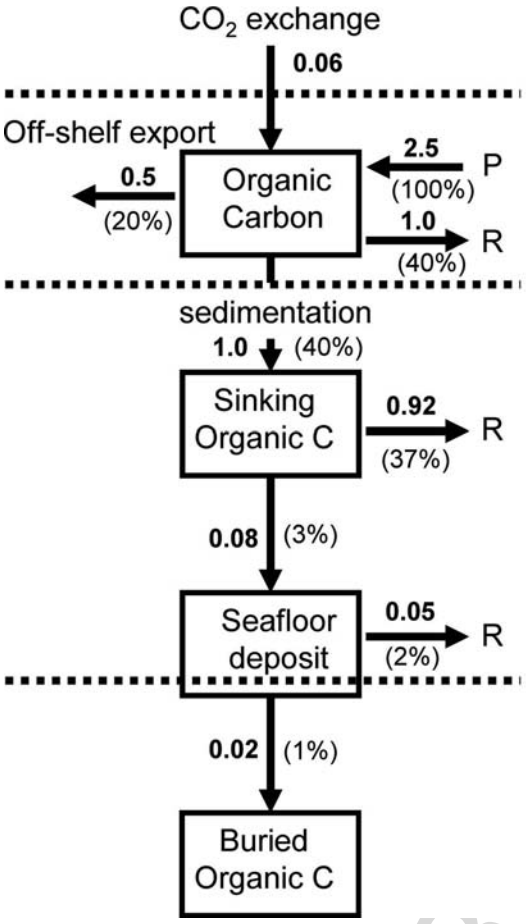

Fig. 2.6.7 Tentative organic carbon budget for the NW Iberian shelf from 42°N to 44°N during the upwelling season. Numbers in $g\,C\,m^{-2}\,d^{-1}$. The air–sea CO_2 flux was derived from the review made in Sect. 2.6.6.3. Adapted from Arístegui et al. (2006)

upwelling was evident from the low temperature and less saline waters over the shelf compared with the adjacent ocean. The distribution of salinity also shows the signature of outwelling from the Rías Baixas (<35.65), which was confined to the inner shelf. There were two distinct hydrographic regions: the Cape Fisterra area (CFA) and the Rías Baixas area (RBA, Fig. 2.6.9). The CFA was characterized by oversaturation of CO_2 and lower temperatures, while the RBA was characterized by under-saturation of CO_2 and higher temperatures. The offshore waters were homogeneously under-saturated of CO_2, although the cool filaments of the CTZ showed lower pCO_2 (Figs. 2.6.8 and 2.6.9). These spatial features were observed during other cruises in the region (June 1997, August 1998 and September 1999) as described by Borges and Frankignoulle (2001, 2002a,b). The fact that the contrast in pCO_2 and temperature between CFA and RBA was observed during all cruises strongly suggests that it is not coincidental but a systematic phenomenon. Lower sea surface temperature in the CFA than in the RBA is a feature that has also been frequently reported in other field studies (e.g. Fraga 1981; Castro et al. 2000; Tenore et al. 1995) or in numerical models (Stevens et al. 2000).

One of the differences between CFA and RBA is the width of the shelf. In the CFA, it varies between 16 and 18 km while in the RBA it is always more than 30 km wide. The ratio between the surface area and the length of the shelf break is 21 ($785\,km^2/37\,km$) and 37 ($3365\,km^2/92\,km$) for CFA and RBA, respectively (Fig. 2.6.9). Since the flushing time of upwelled water is limited by the length of the shelf break, it will be longer in the RBA than in the CFA. This will in turn affect the distribution of surface parameters. We computed theoretically the evolution of surface water temperature and dissolved inorganic carbon (C_T), during the onset of an upwelling event starting from the January 1998 conditions. Figure 2.6.10a shows that in 5 days (the typical duration of the wind stress phase of an upwelling/relaxation cycle in the area) the decrease in surface water temperature related to upwelling is more pronounced in the CFA than in the RBA. The evolution of C_T was computed for two situations: in absence of *NEP* and considering a *NEP* rate of $1.5\,g\,C\,m^{-2}\,d^{-1}$ (see Fig. 2.6.7). Figure 2.6.10b shows that, as expected, surface C_T values increase in relation to upwelling in both areas but the increase in the CFA was more pronounced than that in the RBA, even when taking *NEP* into account. For $NEP = 0$, pCO_2 increases in both areas although more rapidly in the CFA. When considering *NEP*, pCO_2 decreases in the RBA while it remains constant in the CFA (Fig. 2.6.10c). However, the decrease in pCO_2 in the RBA is thermodynamically controlled by the decrease in temperature as shown by the increase of pCO_2 referred to a constant temperature of 16°C (Fig. 2.6.10d). Finally, it should be noted that at the start of the next upwelling cycle, initial pCO_2 and temperature conditions will be different in the two hydrographic regions and, thus, the contrast will be enhanced. These simple computations

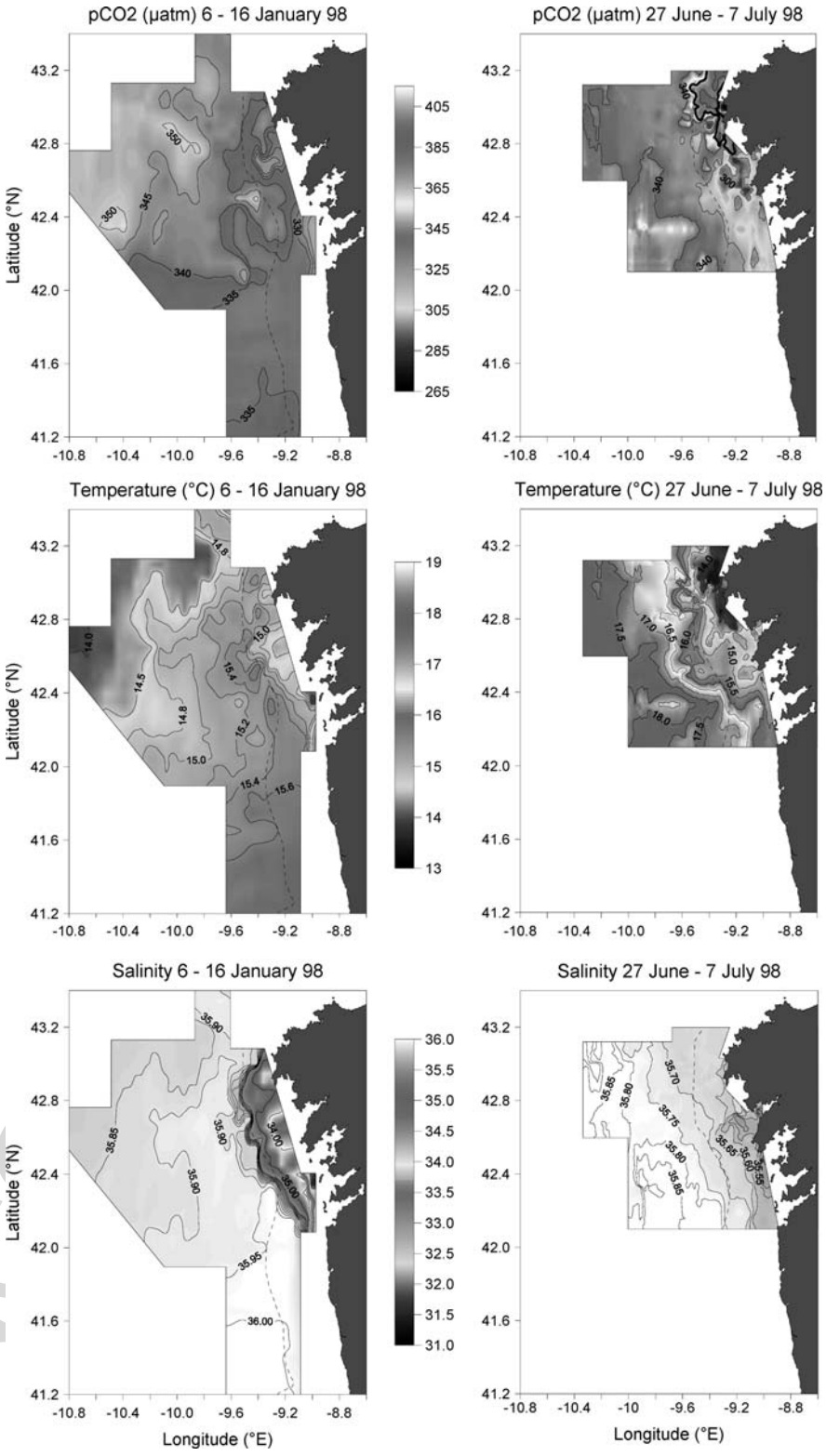

Fig. 2.6.8 Distribution of (**a**) pCO_2 (in µatm), (**b**) temperature (in °C) and (**c**) salinity off the surface waters of the NW Iberian margin in January and July 1998, corresponding, respectively, to downwelling and upwelling conditions (a colored version of this figure is available online; see Appendix C)

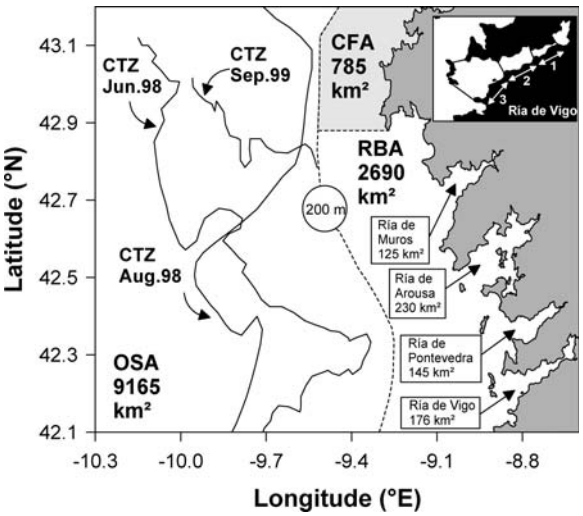

Fig. 2.6.9 Hydrographic regions off the NW Iberian coast: Rías Baixas area (RBA), Cape Fisterra area (CFA), coastal transition zone (CTZ), offshore area (OSA). The insert shows the different sectors of the Ría of Vigo: 1, inner; 2, middle; and 3, outer

illustrate that the observed differences between the two hydrographic areas can, to some extent, be explained by the difference of the width of the shelf. Other processes contribute probably also to enhance upwelling in the CFA. For instance, Haynes et al. (1993) point out the increase of wind stress at Cape Fisterra, due to topographic effects, to explain the distribution of upwelling filaments off the western Iberian coast. Also, off capes, upwelling can occur with a wider range of wind directions than along a linear coastline (Huthnance et al. 2002).

During January 1998, the temperature and salinity distributions were controlled by the WIBP and the IPC (Fig. 2.6.8). As explained in Sect. 2.6.1, the IPC confines the WIBP waters from the rías to the shelf, creating a distinct patch of lower salinity (31.5–35.0) and cooler water (13.7–15.0°C). Under-saturation of CO_2 was observed throughout the sampled region, which can be related to the cooling of surface waters that lowers the pCO_2 values. However, each water mass was characterized by a specific pCO_2 signal. The subtropical ENACW carried by the IPC has lower pCO_2 values (335–340 μatm) than the subpolar ENACW offshore (345–350 μatm), but the lowest values of pCO_2 were associated with the WIBP (315–340 μatm) probably due to enhanced water cooling. This is consistent with the fact that the WIBP is colder than off-shore waters. The mixed layer was shallower over the shelf (60 m) than off-shore (120 m), so that the surface water cooling would be expected to be more important over the shelf. Furthermore, Gago et al. (2003b, c) have shown that the low pCO_2 values observed during winter in the Ría de Vigo are related to the temperature decrease.

Off the Portuguese coast, the few available dissolved inorganic carbon data were acquired in May and December 1993, and August 1994, between 39.8°N and 41.8°N (Pérez et al. 1999). In this area pCO_2 also exhibits strong spatial gradients and the range of values is similar to that off the Galician coast: 320–360 μatm during winter and 320–460 μatm during summer.

2.6.6.2 Distribution of pCO_2 in Surface Waters of the Rías Baixas

Figure 2.6.11 shows transects from the shelf break to the Ría de Vigo itself during the upwelling season. Temperature (Fig. 2.6.11b) was high on 20/06/97 and 09/09/99, which corresponded to upwelling relaxation conditions. The other surveys were conducted under active upwelling conditions of variable intensity. During upwelling relaxation, the influence of the WIBP on the surface salinity distribution is more pronounced than under upwelling conditions. On 20/06/97, the WIBP extends over the entire shelf up to the shelf break. However, even under intense upwelling conditions, there is a signal of the WIBP in the salinity distributions of the ría and the middle shelf.

The distribution of pCO_2 showed a moderate seasonal variability over the outer shelf (range 319–360 μatm) and an intense variability within the ría and the middle shelf (range 250–425 μatm; Fig. 2.6.11c). For a given survey, it is also clear that the distribution of pCO_2 was fairly homogeneous over the outer shelf while exhibiting strong gradients at the vicinity of the ría. In the outer shelf, pCO_2 values were higher on 09/09/99 (relaxation of a strong upwelling event) than on both 20/08/98 and 16/09/99 (strong upwelling events). This is due to the temperature effect on equilibrium constants, because the two transects carried out under strong upwelling events showed higher $pCO_{2(16°C)}$ values than the others (Fig. 2.6.11e). Both pCO_2 and $pCO_{2(16°C)}$ were higher within the ría than over the adjacent shelf on 29/08/98, illustrating the effect of upwelling within the ría. During the two upwelling relaxation events and some of the upwelling events (27/06/98 and 16/09/99), pCO_2 and $pCO_{2(16°C)}$

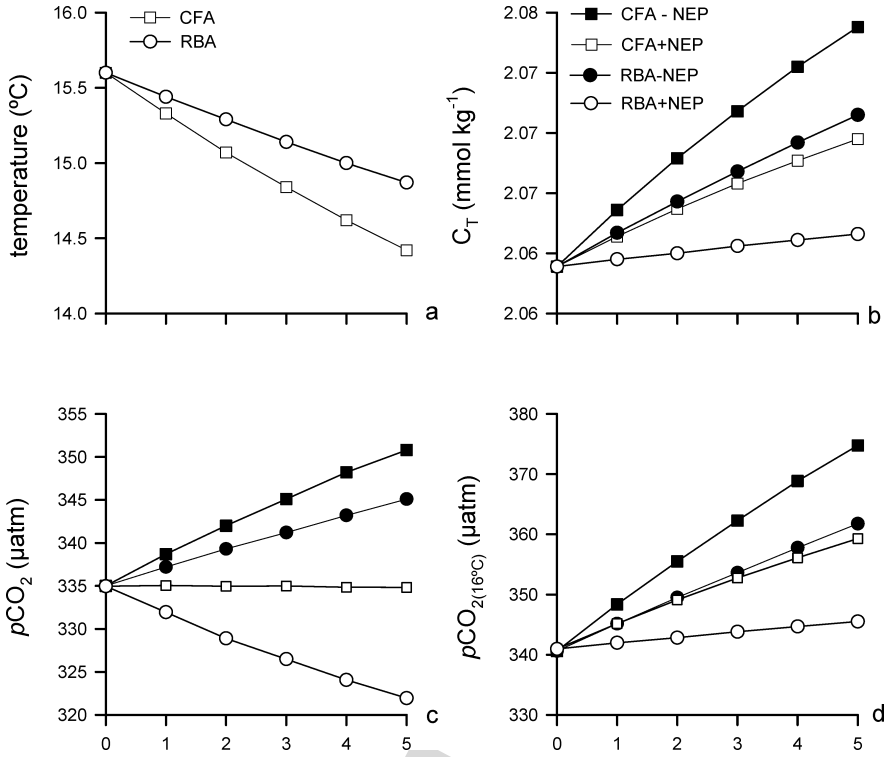

Fig. 2.6.10 Theoretical evolution of (**a**) temperature, (**b**) dissolved inorganic carbon (C_T) (**c**) pCO_2 (in µatm), and (**d**) pCO_2 normalized to 16°C ($pCO_{2(16°C)}$) in the Cape Fisterra (CFA) and the Rías Baixas area (RBA) with the onset of an upwelling event characterized by an offshore Ekman transport values of 750 m^3 s^{-1} (km of coast)$^{-1}$, in the absence of net ecosystem production (*–NEP*) or considering a net ecosystem production of 1.5 g C m^{-2} d^{-1} (*+NEP*). A mixed layer depth of 40 m was considered, and the salinity and total alkalinity (TA) on the shelf and the upwelled water were assumed the same and equal to 35.7 and 2340 µmol kg^{-1}, respectively. We considered that water was upwelled from 150 to 200 m (Huthnance et al. 2002) characterized by pCO_2 = 386 µatm, temperature = 12.0°C and C_T = 2.118 mmol kg^{-1}. The volume of upwelled water was computed using the length of shelf break shown in Fig. 2.6.9 and the upwelling index. The variations of temperature (in °C) and C_T (in mmol kg^{-1}) were computed by iteration during 5 days (half of the typical period of an upwelling cycle) by considering that a volume of shelf surface water is exported, equivalent to the volume of upwelled water, which mixes with water on the shelf. The effect of air–sea exchange of CO_2 on the C_T and pCO_2 (in µatm) was also computed iteratively using the Wanninkhof (1992) gas transfer velocity parameterization, a constant wind speed of 10 m s^{-1} and an atmospheric pCO_2 value of 364 µatm

were lower within the ría than on the adjacent shelf. This is related to *NEP* as corroborated by the distribution $\%O_2$ that shows in general higher values within the ría (Fig. 2.6.11d) and by the good correlation between $pCO_{2(16°C)}$ and $\%O_2$ (Fig. 2.6.11f). It should also be noted that for all surveys $\%O_2$ values were nearly always above the saturation level indicating that during both active upwelling and upwelling relaxation events, *NEP* affected strongly surface parameters and induced the observed under-saturation of CO_2 over the continental shelf (Fig. 2.6.11c).

We can conclude that during both downwelling and upwelling conditions the under-saturation of CO_2 in shelf waters adjacent to the rías is related to *NEP*. During downwelling conditions, the strongly CO_2 under-saturated WIBP outwelled from the rías affects the adjacent continental shelf. However, the outwelling from the rías has little effect on the outer shelf, except during extreme relaxation events. During upwelling conditions, over-saturation of CO_2 is only observed within the rías and CO_2 under-saturation is observed in the adjacent and outer shelf. Even under strong upwelling conditions, *NEP* maintains pCO_2 below the saturation level in the RBA.

Figure 2.6.12 shows the seasonal cycle of pCO_2 in the inner, middle and outer sectors of the Ría de Vigo (sections in Fig. 2.6.9). The three sectors show the same seasonal trends with a distinct decrease in

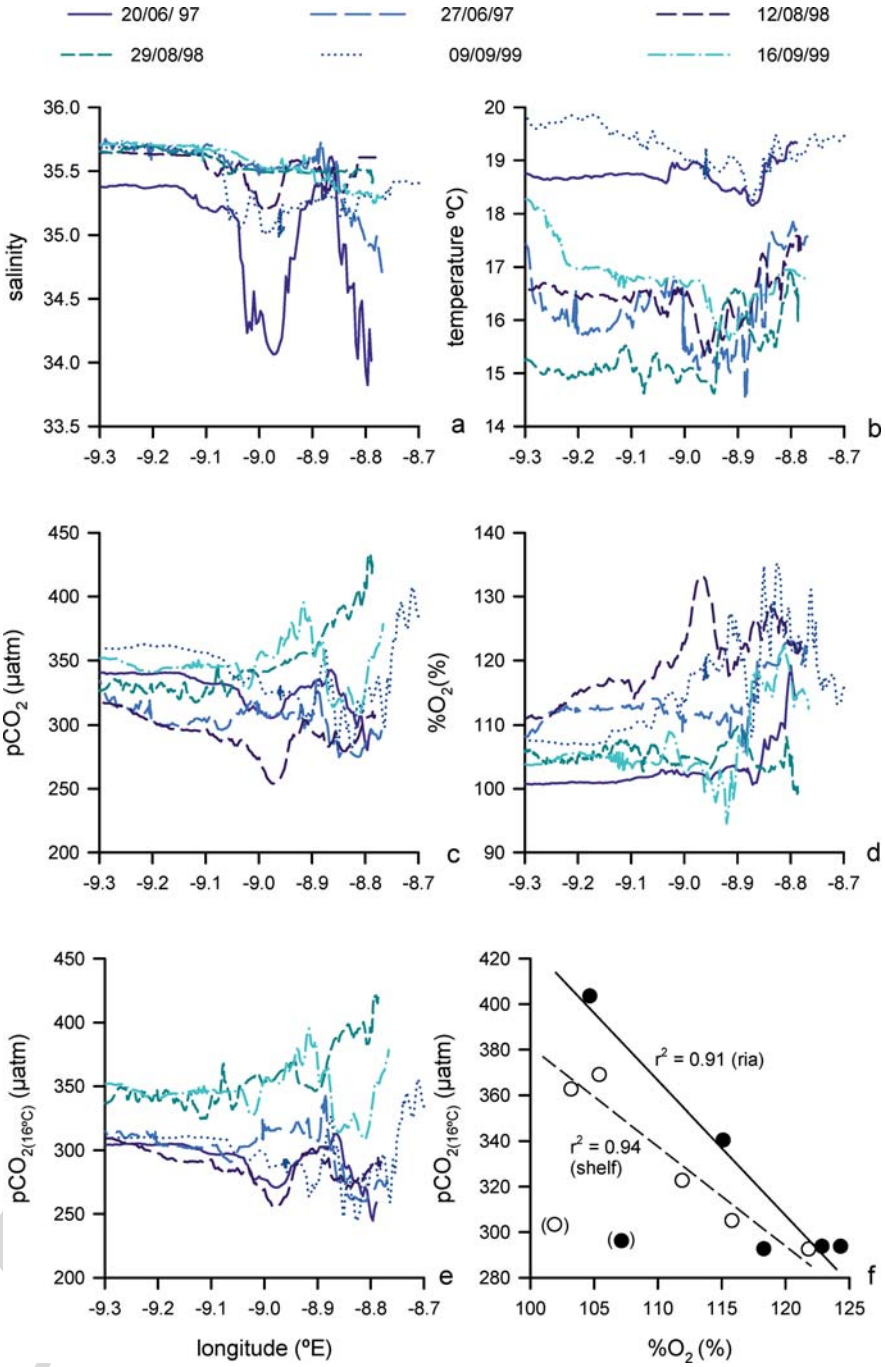

Fig. 2.6.11 Distributions of (**a**) salinity, (**b**) temperature (in °C), (**c**) pCO_2 (in µatm), (**d**) oxygen saturation level ($\%O_2$) and (**d**) pCO_2 normalized to 16°C ($pCO_{2(16°C)}$) along a transect from the shelf break into the Ría de Vigo surveyed six times, and (**e**) average value (for each survey) of $pCO_{2(16°C)}$ versus $\%O_2$. The points in brackets correspond to June 1997 (extreme upwelling relaxation event) and were excluded from the linear regressions. The *horizontal dotted line* is the CO_2 atmospheric equilibrium. The *vertical dotted line* shows the location of the mouth of the Ría of Vigo

pCO_2 from spring to summer, maximal values in late fall and a decrease in winter. Based on the simultaneous application of the non-stationary 2D box model of Eq. (2.6.1) to total alkalinity (TA) and C_T, Gago et al. (2003b) concluded that physical forcing (mostly upwelling/downwelling events) and *NEP* of organic carbon are each responsible for 50% of the 1/2 week variability of pCO_2 in the Ría de Vigo, while *NEP* of calcium carbonate and temperature effects have minimal effects. The seasonal variability of pCO_2 can be attributed to physical forcing, NEP and temperature effects (Borges and Frankignoulle 2002b; Gago

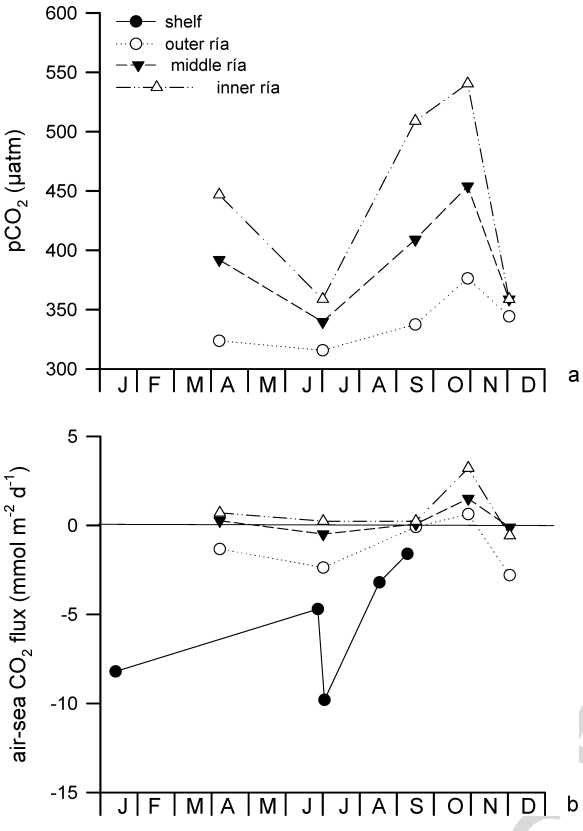

Fig. 2.6.12 Seasonal evolution of (**a**) pCO_2 (in µatm) and (**b**) air–sea CO_2 fluxes (in mmol $C\,m^{-2}\,d^{-1}$) in the Ría de Vigo (based on Gago et al. 2003a) and the rest of the continental shelf (based on Borges and Frankignoulle 2002a). The different sections of the Ría de Vigo are shown in Fig. 2.6.9. The flux values in the Ría de Vigo were converted to the gas transfer velocity parameterization of Wanninkhof (1992) using conversion factors determined from the Rayleigh frequency distribution from values originally computed from the gas transfer velocity parameterization of Woolf and Thorpe (1991)

et al. 2003c). During the upwelling season, CO_2 under-saturation occurs under moderate upwelling or upwelling relaxation conditions due to *NEP*. Under strong upwelling conditions, CO_2 over-saturation is related to the input into the surface layer of aged ENACW enriched in pCO_2 resulting from pelagic and benthic mineralization over the shelf and within the rías (Álvarez et al. 1999; Rosón et al. 1999; Borges and Frankignoulle 2002b; Gago et al. 2003c) as detailed in Sects. 2.6.4.1 and 2.6.5. Net heterotrophy ($Pg < R$) is responsible for the high pCO_2 values in fall, and during winter the low pCO_2 values are related to temperature effects (Gago et al. 2003c). Figure 2.6.12 also shows a distinct increase in pCO_2 from the outer to the inner sector of the ría, which is parallel to the bathymetric gradient. In the shallower (<5 m) inner section (San Simon Bay) enhanced benthic degradation of organic matter leads to the distinct increase in pCO_2 (Gago et al. 2003c).

2.6.6.3 Air–Sea CO_2 Exchange Fluxes

Despite similar averaged pCO_2 values (Fig. 2.6.12), the air–sea CO_2 fluxes are 2–4 times higher over the shelf than into the Ría de Vigo because of the reduced wind speed in the embayment. Table 2.6.1 shows that during the upwelling and the downwelling seasons, the air–sea gradient of CO_2 and the air–sea CO_2 flux are significantly stronger over the continental shelf than in offshore waters. The exception is August 1998, when the CTZ was occupied by an extensive upwelling filament (Fig. 2.6.9), characterized by low pCO_2 values because of strong *NEP* during the early history of the filament (Borges and Frankignoulle 2001). The surface waters of the filaments off the NW Iberian coast are depleted in nutrients and characterized by low primary production (Joint et al. 2001).

Based on the data from Gago et al. (2003c), the air–sea CO_2 flux in the Ría de Vigo is esti-

Table 2.6.1 Air–sea pCO_2 gradient (ΔpCO_2 in µatm) and air–sea CO_2 flux (mmol $C\,m^{-2}\,d^{-1}$) computed using the Wanninkhof (1992) gas transfer velocity parameterization, in the continental shelf (Cape Fisterra area and Rías Baixas area, excluding the Rías) and offshore waters off the Galician coast (adapted from Borges and Frankignoulle 2002a)

		ΔpCO_2 (µatm)		Air–sea CO_2 flux (mmol $C\,m^{-2}\,d^{-1}$)	
		Shelf	Offshore	Shelf	Offshore
21/06–02/07/97	Upwelling relaxation	−34	−23	−4.7	−3.2
27/06–07/07/98	Active upwelling	−38	−22	−9.8	−5.9
11/08–21/08/98	Active upwelling	−11	−19	3.2	−5.5
04/09–11/09/99	Upwelling relaxation	−17	−2	−1.0	−0.1
14/09–18/09/99	Active upwelling	−16	−7	−2.2	−0.9
06/01–19/01/98	Downwelling (winter)	−28	−21	−8.2	−6.0

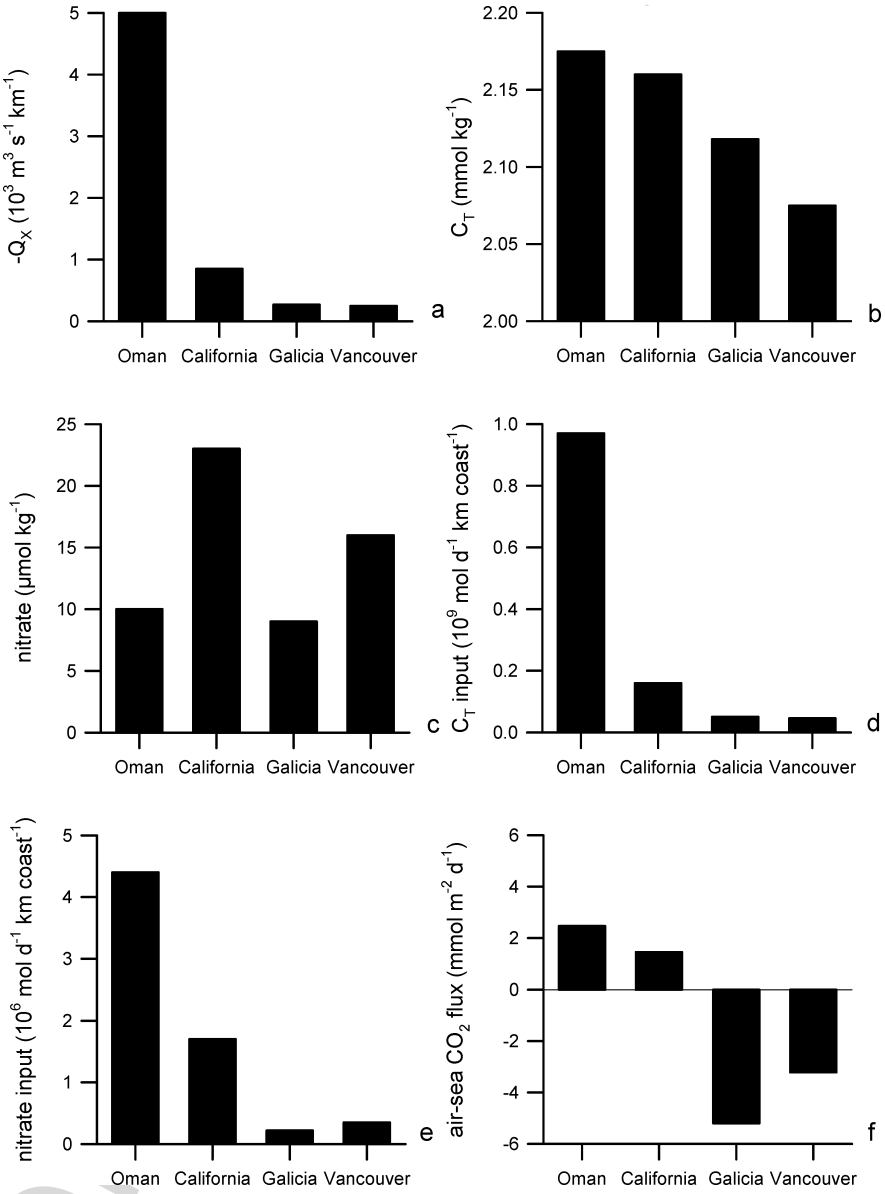

Fig. 2.6.13 Comparison in four coastal upwelling systems (Oman coast, California coast, Galician coast and Vancouver Island coast) of (**a**) offshore Ekman transport (in $m^3\,s^{-1}$ (km of coast)$^{-1}$), (**b**) total dissolved inorganic carbon (C_T, in mmol kg^{-1}) and (**c**) nitrate concentrations (in µmol kg^{-1}) in upwelled water, (**d**) C_T and (**e**) nitrate inputs (in mol d^{-1} (km of coast)$^{-1}$) to the continental shelf and (**f**) air–sea CO_2 fluxes (in mmol C $m^{-2}\,d^{-1}$) over the continental shelf. Data of offshore Ekman transport, C_T and nitrate concentrations for Oman, California and Galician coasts were compiled by Borges (2005) and data for Vancouver Island coast were derived from Ianson et al. (2003). Air–water CO_2 fluxes were compiled by Borges et al. (2005)

mated to be -1.3 and -0.4 mmol C $m^{-2}\,d^{-1}$ during the upwelling and downwelling seasons, respectively. Based on the data in Table 2.6.1, the air–sea CO_2 flux over the continental shelf off the Galician coast is -4.0 and -8.2 mmol C $m^{-2}\,d^{-1}$ during the upwelling and downwelling seasons, respectively (assuming an equal occurrence of active wind stress and relaxation periods during the upwelling season). Assuming that the air–sea CO_2 fluxes of the Ría de Vigo are representative of those for the other Rías Baixas, one can evaluate the air–sea CO_2 flux of the overall NW Iberian coastal upwelling system (CFA + RBA + Rías Baixas), which corresponds to -3.6 and -6.9 mmol C $m^{-2}\,d^{-1}$ during the upwelling and downwelling seasons, respectively. Since the seasonal variability in the NW Iberian upwelling system is mainly bi-modal (upwelling/downwelling seasons), it is reasonable to attempt an annual integration of the air–sea CO_2 fluxes based on data obtained only during summer and winter. Based on the fact that the upwelling season lasts for 7.5 months and the downwelling seasons for 4.5 months (Álvarez-Salgado et al. 2002), the annual air–sea CO_2 flux of the overall NW Iberian coastal upwelling system is esti-

mated to be $-4.8\,\mathrm{mmol\,C\,m^{-2}\,d^{-1}}$. This assessment is close to the one originally computed by Borges and Frankignoulle (2002a) of $-6.1\,\mathrm{mmol\,C\,m^{-2}\,d^{-1}}$ that did not accounted for the air–sea CO_2 fluxes in the Rías Baixas. The annual sink for atmospheric CO_2 in the overall NW Iberian coastal upwelling system is stronger than in the adjacent ocean, estimated to be $-4.1\,\mathrm{mmol\,C\,m^{-2}\,d^{-1}}$ by Borges and Frankignoulle (2002b).

2.6.6.4 Comparison of Air–Sea CO_2 Fluxes with Other Upwelling Systems

Although a relatively abundant literature reporting data of CO_2 dynamics in coastal upwelling systems is available (see review by Borges 2005 and by Borges et al. 2005), air–sea CO_2 fluxes have been calculated just in three other coastal upwelling systems: off the Oman, California and Vancouver Island coasts. The coastal upwelling systems off the Oman and California coasts act as CO_2 sources to the atmosphere, while the coastal upwelling system off the Vancouver Island coast acts as a CO_2 sink. Figure 2.6.13 shows that the two systems that act as CO_2 sources (Oman and California coasts) are characterized by disproportionately higher upwelling indices that lead to much higher inputs of upwelled C_T and nitrate than in the two systems that act as CO_2 sinks (Vancouver Island and W Iberian coast). This could be related to the fact that flushing rates are so high and the nutrients and C_T inputs so intense that exhaustion of nutrients and under-saturation of CO_2 do not occur over the continental shelf in high upwelling index systems, although probably occurring in upwelling filaments. It has also been hypothesized that coastal upwelling systems located at high and mid-latitudes are CO_2 sinks while systems at low latitudes are CO_2 sources (Cai and Dai 2004). However, more data in other systems are required to validate this hypothesis. It has also been argued that the pCO_2 values of upwelled ENACW off the NW Iberian coast are lower (about 400 μatm) compared to aged central waters of the South Atlantic, the Indian and the Pacific Ocean (Arístegui et al. 2006).

AQ34